Structure at Interphase of Poly(vinyl alcohol)−SiC Nanofiber Composite and Its Impact on Mechanical Properties: Positron Annihilation and Small-Angle X-ray Scattering Studies

ARTICLE *in* MACROMOLECULES · AUGUST 2015

Impact Factor: 5.8 · DOI: 10.1021/acs.macromol.5b01095

6 AUTHORS, INCLUDING:

S. K. Sharma
Bhabha Atomic Research Centre
53 PUBLICATIONS **162** CITATIONS
SEE PROFILE

Jyoti Prakash
Bhabha Atomic Research Centre
35 PUBLICATIONS **44** CITATIONS
SEE PROFILE

Debasis Sen
134 PUBLICATIONS **1,057** CITATIONS
SEE PROFILE

Shamsuddin Mazumder
Institute of Advanced Networking Technolog…
163 PUBLICATIONS **1,924** CITATIONS
SEE PROFILE

Macromolecules

Article

pubs.acs.org/Macromolecules

Structure at Interphase of Poly(vinyl alcohol)−SiC Nanofiber Composite and Its Impact on Mechanical Properties: Positron Annihilation and Small-Angle X-ray Scattering Studies

S. K. Sharma,*[,†] J. Prakash,[‡] K. Sudarshan,[†] D. Sen,[§] S. Mazumder,[§] and P. K. Pujari*[,†]

[†]Radiochemistry Division, [‡]Powder Metallurgy Division, and [§]Solid State Physics Division Bhabha Atomic Research Centre, Mumbai 400 085, India

Supporting Information

ABSTRACT: The interphase structure of poly(vinyl alcohol) (PVA)−SiC nanofiber polymer nanocomposites has been investigated using positron annihilation lifetime spectroscopy (PALS) and small-angle X-ray scattering (SAXS). The interphase region in polymer nanocomposites extends from nanofillers' surface to bulk polymer matrix. PVA−SiC nanocomposite films with varying concentration of SiC nanofiber (0.1, 0.2, 0.5, and 1.0 wt %) were prepared using solvent casting method. PALS studies indicated the rearrangement of hydrogen bonded structure of PVA and the creation of an interphase layer with larger size nanoholes. SAXS measurements also confirmed the modification of semicrystalline structure of PVA through lamellae structure parameters. The crystallinity of the nanocomposite films have been determined using X-ray diffraction. The observed changes in the polymer nanocomposite structure are resultant of weak interaction between hydrophilic PVA and hydrophobic SiC nanofiber. The mechanical properties of the nanocomposites measured, using tensile testing method, have been explained in view of the changes in structure at interphase.

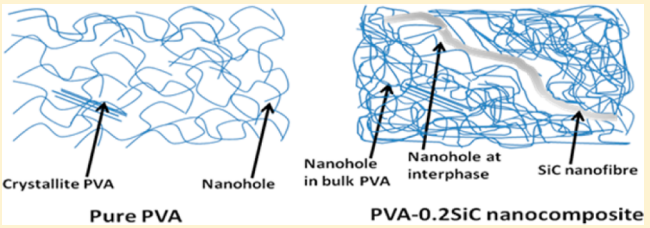

1. INTRODUCTION

Polymer nanocomposites have polymer matrix reinforced with nanosized phase (nanofillers) such as nanoparticles, nanotubes, nanosheets, and nanofibers etc. The physical properties of these composites mainly depend on the interaction between nanofillers and polymer molecules.[1−4] The nanofillers are expected to improve the mechanical properties of the polymer matrix because of higher surface to volume ratio which leads to efficient load transfer from polymer matrix to nanofillers. The higher interfacial energy of nanofillers is expected to provide desirable results by improved bonding between polymer matrix and nanofillers. In this regard, general conclusion from composite theories is that the improved mechanical properties of the nanocomposites are a result of advanced bonding between polymer matrix and the fillers.[5−9] Despite a large number of studies on various types of polymer nanocomposites, no general conclusion has been drawn on structure-mechanical property relationships. This is mainly because different polymer nanocomposites have shown improved as well as worse mechanical properties compared to pure polymer. Among all these studies, a common area of polymer nanocomposite which has attracted enormous attention is a region near interface of polymer matrix and nanofillers viz. interphase.[9−13] The existence of an interphase in large variety of polymer nanocomposites has been inferred through investigation using different structure characterization techniques. The interphase layer extends from surface of nanofillers to deep into bulk polymer matrix. The extension of interphase mainly depends on type, size, and dispersion of nanofillers in polymer matrix. The structure of the interphase layer is different from bulk polymer matrix and it depends on the interaction of nanofillers with polymer molecule as well as on the extension of interphase in polymer matrix.[9,11−14]

The overall properties of polymer nanocomposites heavily depend on the structure of interphase because it controls the load transfer from polymer molecules to the nanofillers. The role of interphase becomes too important because it occupies a substantial volume fraction of bulk polymer matrix e.g. assuming 1 nm thick interphase around nanoparticles can reach 30% of its total volume.[9] The interphase layer has a diffused boundary with bulk polymer phase and hence the effective value of thickness of interphase layer depends on chain flexibility, extent of chain entanglements and the energy of adsorption. The interphase can have a more (less) dense structure compared to polymer matrix if the polymer chain has strong (weak) interaction with the nanofillers.

Several techniques, such as X-ray and neutron scattering, Fourier transform infra-red (FTIR), differential scaling calorimetery (DSC), thermal gravimetric analysis (TGA), and dynamical mechanical analysis (DMA) etc. are employed in an indirect way to infer the structure/properties of interphase in polymer nanocomposites. The electron microscopy techniques

Received: May 22, 2015
Revised: July 6, 2015

DOI: 10.1021/acs.macromol.5b01095
Macromolecules XXXX, XXX, XXX−XXX

have also been used to provide direct structure of the interphase region.

In past few years, our group along with other researchers have shown that positron and triplet state of bound form of positron with an electron (*ortho*-positronium, *o*-Ps) can be used as an efficient probe for investigation of subnanoscopic structure (nanoholes) of interphase in polymer nanocomposites.[15−21] This is possible because positron and *o*-Ps are efficiently trapped in nano sized free volume holes (nanoholes) in polymer matrix. The *pick-off* lifetime (τ_3) of an *o*-Ps atom annihilating from the nanoholes can be correlated to the radius (R) of nanoholes (assuming spherical) through a well established Tao−Eldrup equation.[22,23]

$$\tau_3 = \frac{1}{2}\left[1 - \frac{R}{R + \Delta R} + \frac{1}{2\pi}\sin\left(\frac{2\pi R}{R + \Delta R}\right)\right]^{-1} \quad (1)$$

where ΔR = 0.166 nm is an empirical parameter. The *o*-Ps intensity, I_3, is used to obtain the fractional free volume, and a distribution over *o*-Ps lifetime provides nanoholes size distribution in polymer nanocomposites. Any change in free volume characteristics of polymer matrix as a result of formation of interphase which occupies a substantial volume fraction, is reflected through variations in *o*-Ps lifetime, intensity as well as its distribution. Thus, PALS can provide a more direct measurement of structure at interphase to correlate with the physical properties of polymer-nanocomposites.

In the present study, we have chosen PVA polymer for preparation of nanocomposites owing to its immense applications in fuel cells, coating materials, adhesives, drug delivery and functional membranes due to its unique characteristics namely hydroxyl-rich, water-soluble, biocompatible and nontoxic polymer. Remarkable changes in physical properties like mechanical, thermal and electrical of PVA-based nanocomposites have been reported by incorporating nanofillers having different type of interfacial interaction at molecular level. In the present case, SiC nanofiber has been used as nanofiller to reinforce the PVA matrix. In general, carbon-based nanofillers (carbon nanotubes, graphene oxide, reduced graphene oxide and carbon nanodiamonds etc.) are used to reinforce the polymer matrices. The carbon-based nanofillers are highly conducting which restricts their applications for polymer nanocomposites intended to use in transmission lines, capacitor and electric field grading and linear power electronics etc. SiC nanofibers are wide band semiconductors and will not impart any electrical conductivity to polymer matrix while improving the mechanical properties. SiC nanofibers would only interact with PVA molecules through van der Waals forces (weak interaction) as no direct chemical bonding is possible between SiC and PVA. Hence, in order to avoid the agglomeration of SiC nanofibers into PVA matrix, we have restricted the maximum loading of SiC to 1.0 wt %. PVA−SiC nanocomposite samples containing SiC nanofibers (0.1, 0.2, 0.5, and 1.0 wt %) were prepared using solvent casting method. The interphase structure of the composite samples has been investigated using PALS in view of two layer model (interphase and bulk polymer region) of polymer nanocomposites. The changes in crystallinity of the samples have been investigated using XRD. Thus, determined interphase structure has been correlated to the mechanical properties of the composites measured using tensile testing.

2. EXPERIMENTAL SECTION

2.1. Preparation of SiC Nanofibers. Methyletrichlorosilane (MTS) was procured from Aldrich (99% purity). The SiC nanofibers were synthesized by chemical vapor deposition process using MTS as a precursor. The detailed description of SiC nanofiber preparation has already been reported by us.[24]

2.2. Preparation of PVA−SiC Nanocomposites. PVA (average MW 89000−98000, more than 99% hydrolyzed) and SiC nanofibers were used for the nanocomposite preparation. The synthesized SiC nanofibers were dispersed in deionized (DI) water through long time ultrasonication to obtain a homogeneous dispersion. This suspended solution has shown good stability of SiC nanofiber suspension for a longer duration. For preparation of PVA−SiC nanocomposites, 5 g of PVA was dissolved in 20 mL of DI water at room temperature to form a polymer solution. The SiC suspension was mixed with the polymer solution. The solution was heated to 90 °C under ultrasonication and stirring for 6 h to obtain homogeneous solution. The solution was cast on an extremely cleaned aluminum mold. The composite films were being dried in vacuum at 60 °C for 8 h and stored in desiccator. The different weight percentage (0.1, 0.2, 0.5, 1.0 wt %) of SiC nanofibers was added to obtain the nanocomposite films. These samples are further noted as PVA−*x*SiC, where value of *x* represents the SiC nanofiber weight percent in the nanocomposite films. These films were free from air bubbles and could be taken off easily from the aluminum surface. The thickness of the films was measured to be 100 ± 10 μm using a digital micrometer.

2.3. Characterization of SiC Nanofibers and PVA−SiC Nanocomposites. The microscopic images of SiC nanofibers have been captured using 2000FX JEOL transmission electron microscope and SEM-Camscan MV2300CT/100, UK. The SEM micrograph of fractured surface of PVA−1.0SiC was also taken. X-ray diffraction measurements using Philips X pert pro XRD unit using Cu Kα radiation were carried out to characterize the SiC nanofiber phase and to evaluate the crystallinity of PVA−*x*SiC nanocomposite films.

2.4. Positron Annihilation Measurements. In order to remove any absorbed water from the nanocomposite films, the films were heated at 80 °C for 4 h and stored in a desiccator before carrying out the measurements. The positron annihilation lifetime spectroscopy (PALS) measurements have been carried out at room temperature in laboratory atmosphere. A carrier free NaCl (^{22}Na, 10 μCi) deposited between two 7 μm thick kapton foils was used as positron source. In order to ensure complete positron annihilation within the nanocomposite films, this source was sandwiched between two stacks of the nanocomposite films. A fast−fast coincidence set up coupled to plastic scintillation detectors was used for PALS measurement. The time resolution of lifetime spectrometer was 240 ps and time calibration of MCA was 24.4 ps/channel. All the positron lifetime spectra contained >10^6 counts. Silicon single crystal was used as reference material to estimate the fraction of positrons annihilating within the source (NaCl salt) and kapton foils. The routines PATFIT[25] and CONTIN[26] were used to evaluate the average size, density as well as size distribution of nanoholes in the nanocomposite films.

2.5. Small-Angle X-ray Measurements (SAXS). SAXS measurements were performed on the nanocomposite films using a lab-based SAXS setup having Cu Kα source, and the size of the incident photon beam on the sample was 0.4 mm diameter. The SAXS detector was mounted at a sample-to-detector distance of ∼1.07 m, corresponding to a q-range of 0.1−2.5 nm^{-1}. The scattering intensity was recorded with respect to wave vector transfer, $q = 4\pi\sin(\theta)/\lambda$, where 2θ is scattering angle and $\lambda\sim$ 0.154 nm, the wavelength of probing X-ray.

2.6. Tensile Measurements. Tensile properties of the samples dried under same condition as for positron annihilation and SAXS measurements were determined using a tensile tester, Autograph AGS-1kND (Shimadzu Co.); the initial length of the specimen was 20 mm, and the extension rate was 2 mm/min.

3. RESULTS AND DISCUSSION

3.1. SiC Nanofiber Characterization. Figure 1 shows the XRD pattern of SiC nanofibers. The narrow diffraction peaks

DOI: 10.1021/acs.macromol.5b01095
Macromolecules XXXX, XXX, XXX−XXX

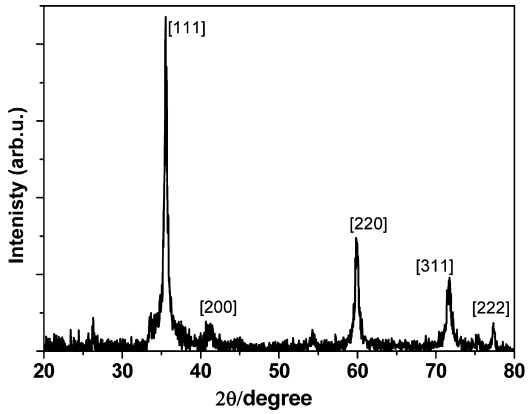

Figure 1. XRD pattern of SiC nanofibers.

corresponding to β-SiC phase indicate the formation of crystalline nanofibers. Figure 2 shows the SEM and TEM

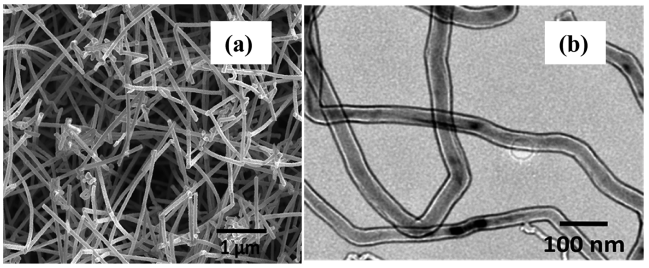

Figure 2. (a) SEM and (b)TEM micrographs of SiC nanofibers.

images of SiC nanofibers. The images show that the diameter of SiC nanofibers is ~50 nm and its length varies on several micrometer length scale. These nanofibers have been incorporated in PVA matrix to form the nanocomposites.

3.2. Nanocomposite Characterization. Figure 3 shows the XRD pattern of pure PVA and PVA−*x*SiC nanocomposites. The characteristic diffraction peak for pure PVA is located at $2\theta \sim 18.5°$. Diffraction peaks corresponding to SiC are not observed in the composite samples probably due to low

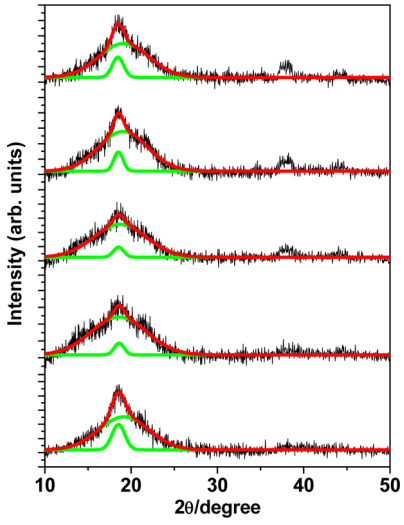

Figure 3. XRD patterns (black lines) of pure PVA and PVA−*x*SiC nanocomposites. The colored lines (red and green) show the fit of diffraction peak to combination of two Gaussian peaks.

concentration of SiC (maximum 1.0 wt %) in PVA matrix. Two new (rather broad and low intensity) diffraction peaks ($\sim 2\theta = 38°$ and 45°) are observed for 0.2−1.0 wt % loading samples. The exact origin of these peaks is unclear to us. PVA is a semicrystalline polymer which shows a characteristic XRD pattern i.e. a narrow peak corresponding to crystallites is overlapped with a broad peak corresponding to amorphous matrix (Figure 3). Any change in the narrow or broad peak's area indicates a relative change in crystallinity of the matrix. In order to evaluate the relative crystallinity, the broad diffraction peak ($2\theta \sim 19°$) is fitted to two Gaussian (narrow and broad) peaks. The ratio of area of the fitted peaks (narrow/broad) is calculated as relative crystallinity of the sample. Thus, calculated relative crystallinity of all the nanocomposites was lower (5.4−13.4%) compared to pure PVA (19.5%).

The reduced crystallinity can be a result of weak interaction of PVA molecules with SiC nanofibers. The presence of SiC nanofibers may act as a physical barrier for long-range ordered arrangement of PVA molecules which in turn will reduce the crystallite size or density of crystallites. This observation is in accordance with our earlier study where a highly ordered arrangement of PVA molecules was observed as a result of strong interaction between PVA molecules and functionalized multiwall carbon nanotubes (*f*MWCNTs).[17] The weak interaction would generally result in an interphase formation with a disrupted hydrogen bonded structure compared to pure PVA.[9] The changes in crystallinity directly influence the mechanical properties of the nanocomposites and worsen of mechanical properties are expected with reduction in crystallinity of a semicrystalline polymer.

3.3. Positron Annihilation Spectroscopy and Small-Angle X-ray Scattering. The discrete positron lifetime components for pure PVA and PVA−*x*SiC nanocomposites are shown in Table 1. The results reported are obtained

Table 1. *o*-Ps Lifetime and Intensity in PVA and PVA−*x*SiC Nanocomposites from PATFIT Analysis and Mechanical Properties Data from Tensile Measurements

sample	*o*-Ps lifetime, τ_3 (ns)[a]	intensity, I_3 (%)[b]	Young's modulus (GPa)	tensile strength (MPa)
pure PVA	1.519	21.5	4.3	77.4
PVA−0.1SiC	1.525	14.2	4.9	107.6
PVA−0.2SiC	1.482	13.6	7.6	79.12
PVA−0.5SiC	1.517	15.2	2.2	79.17
PVA−1.0SiC	1.487	16.0	3.5	62.80

[a]Error ≤ ±0.020 ns. [b]Error ≤ ±0.1%.

keeping all input parameters (lifetimes and their corresponding intensities) free in PATFIT analysis. It is observed that both *o*-Ps *pick-off* lifetime, τ_3, as well as its corresponding intensity, I_3 decreases up to PVA−0.2SiC which further increases on higher loading. In such a case, relative fractional free volume, F_v provides superior information compared to individual parameter (lifetime and intensity) on free volume characteristics of a polymer matrix. F_v is correlated to radius of nanoholes, R (evaluated using eq 1 from *o*-Ps lifetime, τ_3) and corresponding intensity, I_3 (fraction) according to the following empirical equation.[27]

$$F_v = I_3(4\pi R^3/3) \quad (2)$$

DOI: 10.1021/acs.macromol.5b01095
Macromolecules XXXX, XXX, XXX−XXX

The variation of F_v as a function of SiC nanofiber loading is shown in Figure 4. It is observed that F_v shows similar behavior

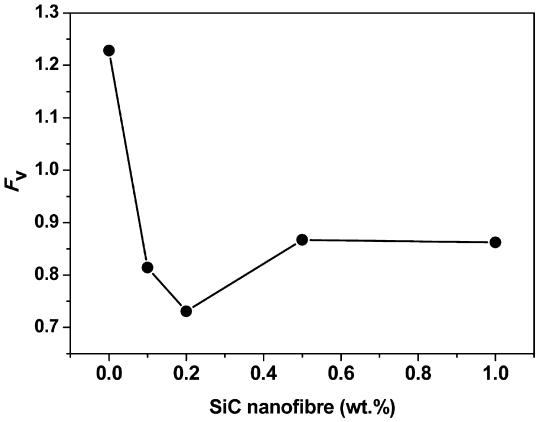

Figure 4. Relative fractional free volume (F_v) in PVA and PVA−*x*SiC nanocomposite determined from PATFIT analysis.

as observed for τ_3; i.e., it decreases from pure PVA to PVA−0.2SiC followed by an increase for higher loading samples. Such a variation in F_v is expected to produce significant changes on the mechanical properties of the nanocomposite films. The discrete component analysis of PALS spectra provides an average picture of free volume nanoholes which surely has a distribution of size in the polymer matrix. In such a case, information about the distribution of nanoholes becomes an important parameter and can be evaluated by measuring the distribution of *o*-Ps lifetime around its mean.

A program, CONTIN is used for this purpose, i.e., to evaluate the distribution of *o*-Ps *pick-off* lifetimes.[26] According to algorithm, the positron lifetime spectrum $s(t)$ is expressed as Laplace transformation of the function $\alpha(\lambda)\lambda$.

Here, $\alpha(\lambda)$ is probability density function of the annihilation rate, λ (inverse of *o*-Ps lifetime) and is expressed by the Gaussian distribution as given by eq 3

$$\alpha_i(\lambda)\lambda \, d\lambda = \frac{1}{\sigma\sqrt{2\pi}} \exp\left[-\frac{(\ln\lambda/\lambda_{i0})^2}{2\sigma^2}\right] d\lambda \tag{3}$$

The subscript i indicates the number of lifetime component and σ gives the standard deviation of the function. In order to evaluate the parameters of these functions, least-squares fitting involving the convolution of resolution function of spectrometer is carried out. Using this approach, the lifetime spectrum is given by the following equation:

$$N(t) = I_1\lambda_1 \exp(-\lambda_1 t) + \sum_{i=2,3} I_i \int_0^\infty \alpha_i(\lambda)\lambda \exp(-\lambda t)\, d\lambda$$
$$\text{with} \sum_{i=1,2,3} I_i = 1 \tag{4}$$

The first expression on the right-hand side is for *para*-positronium (*p*-Ps) which is expected to have a discrete lifetime value (125 ps). Thus, obtained *o*-Ps annihilation rate (lifetime) distribution is transformed to nanoholes radius (eq 5) or nanohole volume distribution (eq 6) through eq 1.

$$n(R) = \frac{2\Delta R}{(R+\Delta R)^2}\left[\cos\left(\frac{2\pi R}{R+\Delta R}\right) - 1\right]\alpha_3(\lambda) \tag{5}$$

$$f(V) = n(R)/4\pi R^2 \tag{6}$$

Thus, evaluated nanoholes radius and nanohole volume distributions are shown in Figures 5 and 6.

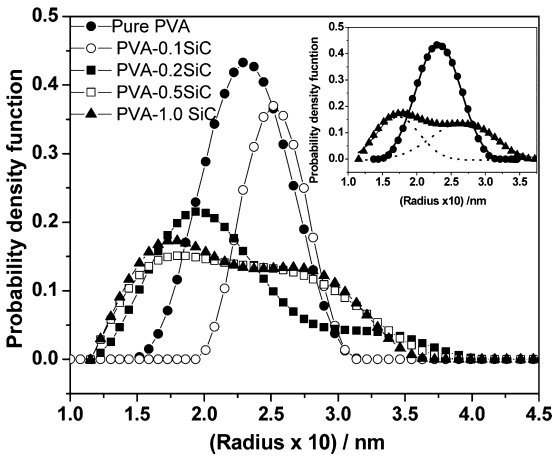

Figure 5. Free volume nanoholes radius distribution in PVA and PVA−*x*SiC nanocomposites. The inset shows the fitting of radius distribution (PVA−1.0SiC) into two Gaussian peaks.

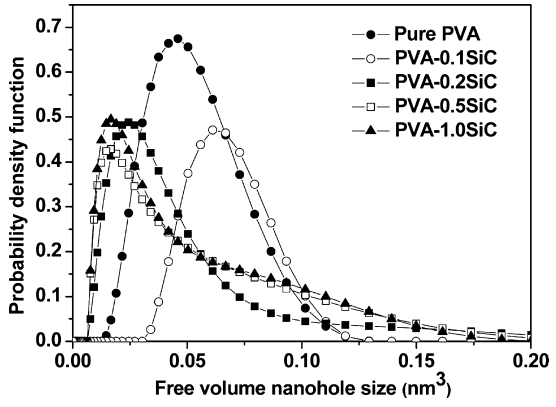

Figure 6. Free volume nanoholes size distribution in PVA and PVA−*x*SiC nanocomposites.

From these figures it is observed that pure PVA and PVA0.1SiC have unimodal nanoholes radius distribution while the higher loading samples (0.2−1.0) have a very broad (approximately bimodal) nanoholes radius (volume) distribution. These type of changes in free volume distribution have also been reported in previous studies on different nanocomposites.[16,17,28] It is to note that lifetime spectrum of PVA−(0.2−1.0)SiC nanocomposites could not be fitted with two *o*-Ps components using PATFIT probably due to broad distribution associated with average *pick-off* lifetimes as seen from decomposition of distribution obtained from CONTIN analysis (Figure 5 and Table 2).

Table 2 shows the average radius $\langle R\rangle$ and fwhm ($w = \sigma$ (2 ln 2)$^{1/2}$) corresponding to the distributions observed in Figure 5. The radius distribution for pure PVA and PVA−0.1SiC were fitted to single Gaussian peak while the distributions for higher loading have been fitted to combination of two Gaussian peaks. Thus, evaluated radius distributions indicate that incorporation of SiC nanofiber in PVA matix not only changes the nanohole size and density but also severely affects the nanoholes size distribution. The observation of bimodal nanoholes size

DOI: 10.1021/acs.macromol.5b01095
Macromolecules XXXX, XXX, XXX−XXX

Table 2. Free Volume Nanoholes Radius Parameters Evaluated from CONTIN Analysis[a])

sample	$\langle R_3 \rangle$ (nm)	w_3 (nm)	$\langle R_4 \rangle$ (nm)	w_4 (nm)	A_3	A_4	relative interphase volume (%)
pure PVA	2.31	0.7754	–	–	0.375 09	0	0
PVA−0.1SiC	2.52	0.5562	–	–	0.228 17	–	–
PVA−0.2SiC	1.95	0.6926	2.90	1.3010	0.175 25	0.077 54	30.9
PVA−0.5SiC	1.68	0.6253	2.55	1.0976	0.088 39	0.185 66	67.7
PVA−1.0SiC	1.72	0.6202	2.65	0.9870	0.128 04	0.159 25	55.4

[a] A_3 and A_4 represent the area under the peak with peak position at $\langle R_3 \rangle$ and $\langle R_4 \rangle$. The relative interphase volume is calculates as $100 \times A_4/(A_3 + A_4)$. The evaluated parameters are result of Gaussian fitting of radius distribution—inset Figure 5.

distribution at higher loading clearly indicate the formation of two spatial zone having different free volume characteristics (Scheme 1.). According to the two layer model of polymer nanocomposites, a region around the nanofillers called interphase (layer 1) is created. The interphase can have more or less dense structure compared to polymer matrix depending on the interaction between polymer molecules and nanofillers. The adsorption of polymer chains also affect their entanglement and this effect can even propagate to bulk matrix resulting in variation of free volume characteristics of bulk polymer phase (layer 2) present in polymer nanocomposites. PVA is a hydrophilic polymer having a hydrogen bonded network. The hydrogen bonding network of PVA basically governs the crystallinity as well as free volume properties of the polymer which in turn determine the physical properties of the polymer. We have shown in previous studies that on incorporation of *f*MWCNTs, the crystallinity of PVA matrix is improved as a result of formation of an ordered arrangement of PVA molecules on *f*MWCNTs surface. This ordered arrangement is formed because *f*MWCNTs provides a large number of interaction points at its surface through amino group which can bond with the −OH group of the PVA molecule through covalent and hydrogen bonding.[17] In this study, it was also shown that as a result of PVA and *f*MWCNTs interaction, the complete hydrogen-bonded structure of PVA is modified resulting in different free volume characteristics than pure PVA.

In the present study, we have used SiC nanofibers which can enhance the mechanical properties of the PVA as a result of load transfer from PVA molecules to SiC nanofibers without imparting any electrical conductivity. As SiC nanofibers have hydrophobic surface and do not interact directly with PVA molecules through chemical bonding, the only way of interaction is van der Waals forces. As mentioned before, SiC nanofiber being hydrophobic in nature will start aggregating in the polymer matrix at higher concentration and hence we have restricted the SiC loading to very low level (highest loading = 1.0 wt %, Figure S1,Supporting Information). According to the two layer model, a less dense (large free volume) interphase layer formation is plausible in the studied nanocomposites because of weak interaction between SiC nanofibers and PVA molecules. The SiC nanofibers will act as a physical barrier to PVA molecules and disorganize the molecular morphology. At lowest loading, the radius distribution does not really indicate the existence of a zone with different free volume characteristics. On the other hand, an increase in nanoholes size (*o*-Ps lifetime) with lower nanoholes density (less intensity) compared to pure PVA is observed for the lowest loading sample (PVA0.1SiC). This indicates a change in the hydrogen bonded structure of PVA throughout the matrix and no clear boundary for interphase in this sample. The plausible reasons for not observing a bimodal (or very broad) distribution can be a diffused boundary of interphase or smaller volume fraction occupied by the interphase layer. However, the interphase volume for this sample is expected to be lower than PVA0.2SiC. At higher loadings, a broader nanoholes radius distribution has been observed wherein the peak corresponding to higher mean value of nanoholes radius $\langle R_4 \rangle$ can be assigned to the interphase layer (Table 2). The relative interphase volume fraction has been estimated by taking ratio of area corresponding to $\langle R_4 \rangle$ peak to the total area. Thus, calculated values of relative interphase volume fraction are also mentioned in Table 2. It is also observed that nanoholes radius corresponding to polymer bulk matrix (layer 2) in nanocomposites is lower than pure PVA. This indicates that formation of interphase layer also affects the hydrogen bonded structure of PVA matrix in bulk phase as represented in Scheme 1.

The SAXS profiles, in double logarithmic scale, are shown in Figure 7. It is evident from the typical feature of the SAXS data that scattering profiles of the composite samples can be divided into two zones, zone-I and zone-II. With increase in SiC

Scheme 1. (A) Free Volume Nanoholes in Pure PVA (B) PVA−0.2SiC Nanocomposite Structure Having Two Layers, viz. Interphase Region with Larger Size Nanoholes and Bulk Region with Smaller Size Nanoholes Compared to Pure PVA

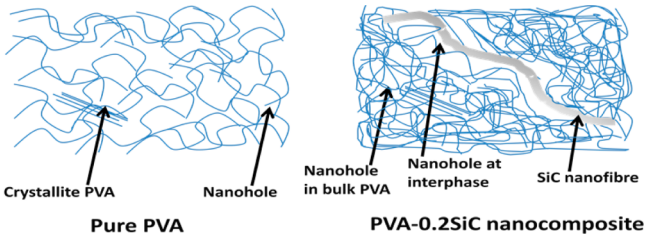

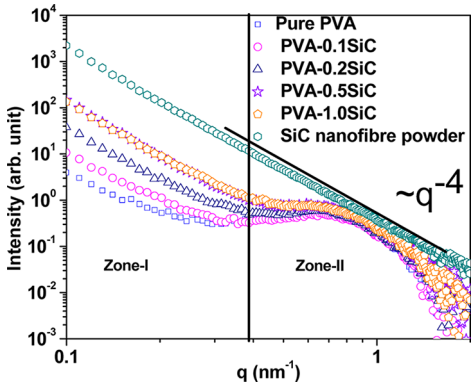

Figure 7. SAXS profile of the samples in double logarithmic scale. Only $^1/_5$th of the data points are shown to enhance the clarity of the figure.

DOI: 10.1021/acs.macromol.5b01095
Macromolecules XXXX, XXX, XXX−XXX

nanofiber content, zone-I is modified significantly. The functionality of zone-I mimics that of the SiC. Zone-II of the scattering profiles mainly contains the information about the PVA matrix and its modification with increase in SiC nanofiber content. In the present work, our primary focus has been to investigate the modification of the nanostructure of the PVA matrix as a function of SiC concentration. In order to investigate this effect, SAXS data were analyzed using the Hosemann model.[29] In light of this model, the scattering intensity from PVA polymer is given by

$$I_{PVA}(q) = \frac{I_0}{q^4}\exp(-\sigma_{el}{}^2q^2)\,\mathrm{Re}\left[\frac{(1-f_c(q))(1-f_a(q))}{[1-f_c(q)f_a(q)]}\right] \quad (7)$$

where I_0 is a constant and the exponential term in the numerator accounts for the changes in the SAXS intensity profile caused by a transition layer between crystalline and amorphous regions. The parameter σ_{el} characterizes a sigmoidal electron density profile in the layer. The parameters $f_c(q)$ and $f_a(q)$ are the Fourier transforms of the thickness distribution functions.

$$f_c(q) = \exp(il_cq)\exp\left(\frac{-\sigma_c{}^2q^2}{2}\right)f_a(q)$$

$$= \exp(il_aq)\exp\left(\frac{-\sigma_a{}^2q^2}{2}\right)$$

Here, l_c and l_a correspond to the thicknesses of the crystalline lamellae and amorphous layers, respectively. The average long period L_p can be simply deduced by $L_p = l_c + l_a$. To take into account the scattering contributions from the composite consisting of both PVA and SiC nanofiber, the total scattering intensity was expressed as

$$I_{tot}(q) = I_{PVA}(q) + wq^{-n} \quad (8)$$

The second term (wq^{-n}) takes care of the scattering contribution from the SiC nanofibers present in the nanocomposites.

The parameters were extracted by fitting the above model to the experimental scattering profiles using nonlinear least-square method. The extracted parameters are tabulated in the Table 3.

Table 3. Extracted Parameters Obtained from SAXS Analysis

sample	l_c (nm)	σ_c (nm)	l_a(nm)	σ_a(nm)	w/I_0 (10^{-3})	n
pure PVA	4.9	2.34	2.8	0.09	0.0	–
PVA–0.1 SiC	4.7	2.79	2.3	0.07	5.5	4
PVA–0.2 SiC	4.7	2.72	2.3	0.08	32.0	4
PVA–0.5 SiC	4.7	2.60	2.3	0.08	104.0	4
PVA–1.0 SiC	4.7	2.64	2.4	0.09	104.0	4

The fit of the model and the data is shown in the Figure 8 through Kratky plots ($I(q)q^2$ vs q). It is observed from the fitted parameters that PVA has a lamellae structure which is modified on nanocomposite formation. The thickness of crystalline lamellae and amorphous layer are observed to decrease on composite formation (see the changes from pure PVA to PVA0.1SiC) which remains nearly constant throughout the studied SiC content. The results indicate that the lamellae structure of PVA at nanometer scale does not change significantly on incorporation of varying concentration of SiC

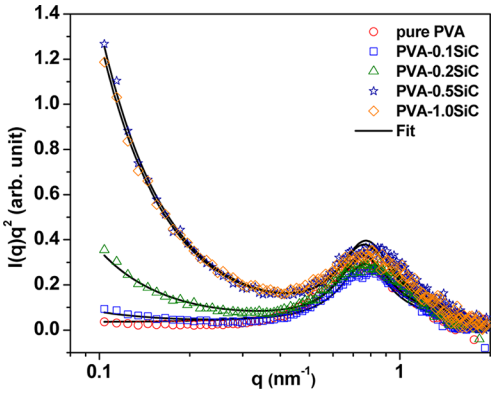

Figure 8. Fit of the model, as mentioned in the text, to the scattering profiles. Only $^1/_5$th of the data points are shown for clarity of the figure.

nanofiber from 0.1 to 1.0 wt %. However, it is to be noted that significant changes have been observed at subnano level (nanoholes size, density and size distribution) structure using positronium probe through the studied concentration range of SiC nanofiber.

3.4. Interphase Structure and Mechanical Properties.

In order to evaluate the role of interphase structure on mechanical properties of polymer nanocomposites, tensile measurements have been carried out and reported in Table 1. The results show that the Young's modulus for nanocomposites increases up to 0.2% loading and starts reducing with further loading (Figure 9). According to conventional theories of

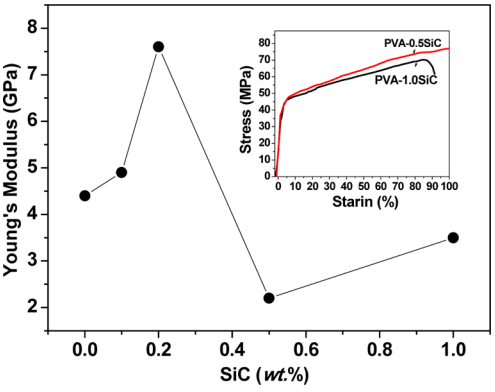

Figure 9. Young's modulus of PVA–xSiC nanocomposites as a function of SiC nanofibers loading. The inset shows the stress–strain curves for the PVA–xSiC (x = 0.5 and 1.0) composites.

polymers, the fractional free volume should be lower for better mechanical properties. This happens because the presence of nanoholes reduces the efficiency of load transfer among polymer molecules. It can be seen from Figure 4 that F_v decreases up to 0.2% loading followed by an increases with further loading. This indicates that the variation of Young's modulus in the studied nanocomposite can be inversely correlated to the fractional free volume (F_v, Figure 4) measured through discrete PALS analysis without invoking the nanoholes radii distributions. It is to note that the variations in Young's modulus and F_v cannot be linearly correlated due to presence of SiC. The tensile strength of the nanocomposite is observed to be lower than pure PVA except the lowest loading sample

DOI: 10.1021/acs.macromol.5b01095
Macromolecules XXXX, XXX, XXX–XXX

indicating that the nanocomposites are less ductile than pure PVA (Table 1).

In view of interphase formation and its structure, the mechanical properties of nanocomposites will depend on various factors such as nanofillers content, load transfer mechanism between polymer molecule and nanofillers, interphase volume fraction, interphase structure and resultant bulk polymer matrix structure. In the present case, it appears that up to 0.2% loading, only nanofiber content remains important factor as interphase volume remains low e.g. for PVA(0.1−0.2)SiC samples the relative interphase volume is ≤30.9% (Table 2). At 0.5 wt % concentration, the relative interphase volume increases to 67.7% which diminishes the load transfer between PVA molecules and SiC. At 1.0% loading, the relative interphase volume (55.4%) does not further increase probably due to some agglomeration of SiC nanofibers which consequently further restricts the reduction in Young's modulus of the nanocomposites.

It is to be noted that in case of semicrystalline polymers, crystallinity plays important role toward mechanical strength. Several studies on PVA nanocomposite have shown the improvement in its mechanical properties.[17,30−32] In these studies, it remained a conjecture if the enhancement in mechanical properties is resultant of load transfer from molecules to nanofillers or due to enhancement in crystallinity. The PVA−*x*SiC nanocomposites have shown variation in mechanical properties (Young's modulus) with detriment in crystallinity and paved the way for understanding the impact of interphase structure on mechanical properties.

4. CONCLUSION

The interphase of PVA−SiC nanofiber composites has been characterized to explore the correlation of its structure with mechanical properties. The weak interaction between hydrophobic SiC nanofiber and hydrophilic PVA resulted in a low density (more free volume) interphase region as observed through positronium probe. No significant changes were observed in lamellae structure of PVA with increased SiC nanofiber concentration. Incorporation of SiC nanofibers in PVA could improve the mechanical properties (Young's modulus and yield strength) at lower concentration (up to 0.2 wt %). At higher SiC concentration, the mechanical properties are deteriorated due to formation of the low density interphase which makes load transfer inefficient from PVA matrix to SiC nanofiber. In order to further improve the mechanical properties of the composites, it is proposed to enhance interaction between SiC and PVA through surface modifications of SiC nanofibers by hydrophilic functional groups.

■ ASSOCIATED CONTENT

Ⓢ Supporting Information

The Supporting Information is available free of charge on the ACS Publications website at DOI: 10.1021/acs.macromol.5b01095.

SEM micrograph of fractured surface of PVA0.1SiC (PDF)

■ AUTHOR INFORMATION

Corresponding Authors

*(P.K.P.) E-mail: pujari@barc.gov.in. Fax: (91)-22-2550-5151.
*(S.K.S.) E-mail: skumars@barc.gov.in.

Notes

The authors declare no competing financial interest.

■ REFERENCES

(1) Wong, M.; Tsuji, R.; Nutt, S.; Sue, H.-J. *Soft Matter* **2010**, *6*, 4482−4490.
(2) Kim, S. Y.; Schweizer, K. S.; Zukoski, C. F. *Phys. Rev. Lett.* **2011**, *107*, 225504.
(3) Maillard, D.; Kumar, S. K.; Fragneaud, B.; Kysar, J. W.; Rungta, A.; Benicewicz, B. C.; Deng, H.; Cate Brinson, L.; Douglas, J. F. *Nano Lett.* **2012**, *12*, 3909−3914.
(4) Deng, F.; Ito, M.; Noguchi, T.; Wang, L.; Ueki, H.; Niihara, K.-I.; Kim, Y. A.; Endo, M.; Zheng, Q.-S. *ACS Nano* **2011**, *5*, 3858−3866.
(5) Chan, C.-M.; Wu, J.; Li, J.-X.; Cheung, Y.-K. *Polymer* **2002**, *43*, 2981−2992.
(6) Gersappe, D. *Phys. Rev. Lett.* **2002**, *89* (5), 058301.
(7) Reynaud, E.; Jouen, T.; Gauthier, C.; Vigier, G.; Varlet, J. *Polymer* **2001**, *42*, 8759−8768.
(8) Shelley, J. S.; Mather, P. T.; DeVries, K. L. *Polymer* **2001**, *42*, 5849−5858.
(9) Ciprari, D.; Jacob, K.; Tannenbaum, R. *Macromolecules* **2006**, *39*, 6565−6573.
(10) Kovacevic, V.; Lucic, S.; Leskovac, M. *J. Adhes. Sci. Technol.* **2002**, *16*, 1343−1365.
(11) Tannenbaum, R.; Zubris, M.; David, K.; Ciprari, D.; Jacob, K.; Jasiuk, I.; Dan, N. *J. Phys. Chem. B* **2006**, *110*, 2227−2232.
(12) Sen, S.; Xie, Y.; Kumar, S. K.; Yang, H.; Bansal, A.; Ho, D. L.; Hall, L.; Hooper, J. B.; Schweizer, K. S. *Phys. Rev. Lett.* **2007**, *98*, 128302.
(13) Coiai, S.; Prevosto, D.; Bertoldo, M.; Conzatti, L.; Causin, V.; Pinzino, C.; Passaglia, E. *Macromolecules* **2013**, *46*, 1563−1572.
(14) Papon, A.; Montes, H.; Hanafi, M.; Lequeux, F.; Guy, L.; Saalwachter, K. *Phys. Rev. Lett.* **2012**, *108*, 065702.
(15) Sharma, S. K.; Prakash, J.; Sudarshan, K.; Maheshwari, P.; Sathiyamoorthy, D.; Pujari, P. K. *Phys. Chem. Chem. Phys.* **2012**, *14*, 10972−10978.
(16) Sharma, S. K.; Bahadur, J.; Patil, P. N.; Maheshwari, P.; Mukherjee, S.; Sudarshan, K.; Mazumder, S.; Pujari, P. K. *ChemPhysChem* **2013**, *14*, 1055−1062.
(17) Sharma, S. K.; Prakash, J.; Bahadur, J.; Sudarshan, K.; Maheshwari, P.; Mazumder, S.; Pujari, P. K. *Phys. Chem. Chem. Phys.* **2014**, *16*, 1399−1408.
(18) Patil, P. N.; Sudarshan, K.; Sharma, S. K.; Maheshwari, P.; Rath, S. K.; Patri, M.; Pujari, P. K. *ChemPhysChem* **2012**, *13*, 3916−3922.
(19) Harms, S.; Ratzke, K.; Faupel, F.; Schneider, G. J.; Willner, L.; Richter, D. *Macromolecules* **2010**, *43*, 10505−10511.
(20) Zaleski, R.; Kierys, A.; Grochowicz, M.; Dziadosz, M.; Goworek, J. *J. Colloid Interface Sci.* **2011**, *358*, 268−276.
(21) Awad, S.; Chen, H.; Chen, G.; Gu, X.; Lee, J. L.; Abdel-Hady, E. E.; Jean, Y. C. *Macromolecules* **2011**, *44*, 29−38.
(22) Tao, S. J. *J. Chem. Phys.* **1972**, *56*, 5499−5510.
(23) Eldrup, M.; Lightbody, D.; Sherwood, J. N. *Chem. Phys.* **1981**, *63*, 51−58.
(24) Prakash, J.; Ghosh, S. K.; Sathiyamoorthy, D.; Venugopalan, R.; Paul, B. *Curr. Nanosci.* **2012**, *8*, 161−169.
(25) Provencher, S. W. *Comput. Phys. Commun.* **1982**, *27*, 213−227.
(26) Kirkegaard, P.; Eldrup, M. *Comput. Phys. Commun.* **1974**, *7*, 401−409.
(27) Jean, Y. C., Mallon, P. E., Schrader, D. M., Eds. *Principles and Applications of Positron and Positronium Chemistry*; World Scientific: London, 2003.
(28) Zhou, W.; Wang, J.; Zhenli, G.; Gong, J.; Qi, N.; Wang, B. *Appl. Phys. Lett.* **2009**, *94*, 021904.
(29) Hosemann, R.; Bagchi, S. N. *Direct Analysis of Diffraction by Matter*; North Holland: Amsterdam, The Netherlands, 1962.
(30) Liu, L. Q.; Barber, A. H.; Nuriel, S.; Wagner, H. D. *Adv. Funct. Mater.* **2005**, *15*, 975−980.
(31) Morimune, S.; Kotera, M.; Nishino, T.; Goto, K.; Hata, K. *Macromolecules* **2011**, *44*, 4415−4421.

DOI: 10.1021/acs.macromol.5b01095
Macromolecules XXXX, XXX, XXX−XXX

(32) Zhao, X.; Zhang, Q. H.; Chen, D. J.; Lu, P. *Macromolecules* **2010**, *43*, 2357−2363.

DOI: 10.1021/acs.macromol.5b01095
Macromolecules XXXX, XXX, XXX−XXX